Atmospheric transport and deposition of microplastics in a remote mountain catchment

Steve Allen, Deonie Allen, Vernon Phoenix, Gaël Le Roux, Pilar Durántez Jiménez, Anaëlle Simonneau, Stéphane Binet, Didier Galop

Atmospheric transport and deposition of microplastics in a remote mountain catchment

Steve Allen[ŧ a,b], Deonie Allen[ŧ*a], Vernon R. Phoenix[b], Gaël Le Roux[a], Pilar Durantez[a], Anaëlle Simonneau[c], Stéphane Binet[a,c], Didier Galop[d]

[a] EcoLab (Laboratoire Ecologie Fonctionnelle et Environnement), ENSAT, UMR-CNRS 5245, Castanet Tolosan (France)

[b] Department of Civil and Environmental Engineering, University of Strathclyde, Glasgow, G1 1XQ, Scotland, UK

[c] ISTO, CNRS UMR 7327, Université d'Orléans, BRGM (France)

[d] GEODE, UMR-CNRS 5602, Université Toulouse Jean Jaurès (France)

[ŧ] joint first authors (S Allen: https://orcid.org/0000-0002-2333-6514; D Allen: https://orcid.org/0000-0002-4038-9394)

[*] corresponding author: deonie.allen@ensat.fr; deoniea@gmail.com

Abstract

Plastic litter is an ever-increasing global issue and one of this generation's key environmental challenges. Microplastics have reached oceans via river transport on a global scale, but outside two mega-cities, Paris (France) and Dongguan (China), there is a lack of information on atmospheric microplastic deposition or transport. Here we present the observations of atmospheric microplastic deposition in a remote, pristine, mountain catchment (French Pyrenees). We analyse five months of samples representing atmospheric wet and dry deposition and identify fibres up to ~750 µm long and fragments ≤300µm as microplastics. We document relative daily counts of 249 fragments, 73 films and 44 fibres per square metre depositing on the catchment. Air mass trajectory analysis shows microplastic

transport through the atmosphere over a distance of up to 95km. We suggest that microplastics can reach and affect remote, sparsely inhabited areas through atmospheric transport.

Key words: microplastic, atmospheric fallout, aerosol plastic, remote area.

Main text

Plastic industry experts estimate global manufacture of 335 million tonnes (Mt) of plastic in 2016[1]. Of the 335Mt worldwide, 60Mt was produced in Europe, of which ~40% is packaging (short-term or single use). However, in 2016 27.1Mt was recovered as waste for recycling, energy recovery (burning) or placed in landfill[2,3]. Some plastics remain in service for up to 50 years, which helps explain some of the 32.9Mt discrepancy in the plastics mass balance. While plastic is recognised to biodegrade very slowly, degradation to micro (5mm-1µm) and nanoplastics (<1µm) does occur[4,5]. Thus, plastic waste can start as macroplastic pieces (bottles, packaging etc.) and over time degrades to microplastic (MP) particles or smaller. Mattson et al.[6] estimate 10% of created plastics enter the ocean annually, accounting for a portion of the 32.9Mt plastics waste. However, this highlights questions on the fate of the remaining plastic. Large amounts of macroplastic waste would be noticed in the terrestrial environment, but if this waste was degraded to micro-sized particles it could evade easy detection. Recent studies have identified MP on alpine river floodplains[7] and lake sediment[8] illustrating terrestrial MP occurrence, and in mega-cites as aerosol pollution[9–12]. The recent research on atmospheric fallout in Paris (France)[9–11] and Dongguan (China)[12] suggests atmospheric MP conveyance and corresponding deposition. Soil/sediment/lake samples provide an informative terrain-based analysis of plastic[7,13–16] occurrence however

47 determination of atmospheric MP beyond intra-city deposition requires source specific and
48 remote atmospheric sampling.

49 This research provides unequivocal evidence of direct atmospheric fallout of MP in a remote
50 area of the Pyrenees Mountains. The Pyrenees mountainous regions are anecdotally
51 considered pristine wilderness due to limited development, difficulty of human access and
52 distance from major populations or industrial centres. The study site is located at the
53 Bernadouze meteorological station[17], 42°48'14.6"N 1°25'06.8"E and 1425m a.s.l., within the
54 Vicdessos catchment and Mid-Pyrenees mountains in south-west of France (Supplementary
55 Note 1 - Detailed site description). The local vicinity is sparsely populated, without industrial,
56 commercial or large agricultural activities and is primarily used for recreational activities
57 (hiking, skiing, environmental education and scientific research). The closest local residential
58 area is a village ~6km to the south-east (Vicdessos village, population ~540[18]) with a
59 moderately sized town located ~25km to the north-east (Foix, population ~9,720[18]).

60 The presented research considers five months of atmospheric deposition collected from the
61 field site. Five samples of total atmospheric deposition (wet and dry), from two separate
62 monitoring devices, were analysed to identify if MPs are present in the remote mountain
63 catchment. Regular (monthly) sampling campaigns were proposed, however weather
64 conditions restricted site access resulting in irregular monitoring intervals (Methodology,
65 Supplementary Table 1). The objective in observing the case study atmospheric deposition
66 was to identify (1) if MPs are present in atmospheric fallout in this remote mountainous
67 location and (2) if MP are present, in what quantity, size, shape and plastic type do they
68 occur? The purpose of this study was to take steps towards discovering the extent of MP
69 atmospheric deposition in remote terrestrial locations.

MP particles in the remote mountain catchment

MP fragments, fibres and films were found, and confirmed (through visual microscopy inspection and μRaman analysis[19]) in all atmospheric deposition samples collected from the field site. This illustrates that for this location there is an atmospheric MP presence. The atmospheric MP deposition captured in the collectors are presented in Figure 1.

Figure 1 near here

Details of local meteorological conditions recorded at the sampling site are provided in Supplementary Table 1 in conjunction with normalised MP counts (MP/m^2/day) per day. The meteorological record illustrates lower relative precipitation and fewer storms (rain or snow) in November compared to the following months. The relative snowfall increased over the monitoring period while rainfall was greatest in the January. Monthly average wind speed fluctuated around 1.1(±0.6)m/s with a maximum recorded wind speed of 7.1m/s in December. December-March illustrate wind speeds >4m/s and the greatest relative number of wind events (>2m/s and >3m/s) occurred in March. The number of >1m/s events were greatest in November and March, declining to the lowest frequency in February.

Field sample MP counts illustrate an average daily particle deposition of 365/m^2/day (±69, standard deviation). Sample MP counts were normalised to represent daily atmospheric deposition (MP/m^2/day) as site access limitations resulted in inconsistent monitoring durations (November extended 12 days, December 19 days, January and March 34 days, February 41 days).

Both rainfall and snowfall show moderate to strong significant correlations with MP count in the original dataset ($r \geq 0.8$, $p < 0.05$) and to the monitoring duration (days) (Supplementary Note 2). The normalised dataset presents a positive correlation to the frequency of wind

speeds >1m/s (light air-strong wind movement) ($r>0.8$, $p<0.05$) suggesting MP transport and deposition may be influenced by wind movement. The maximum rainfall intensity also presents a strong positive correlation ($r>0.9$, $p<0.05$) suggesting that individual events and the intensity of events may influence atmospheric MP deposition (scavenging)[20]. While it is acknowledged that the dataset is limited, the number of snowfall events also shows a positive correlation with normalised MP deposition ($r\geq0.6$, $p<0.05$). The duration (average and maximum) of both rainfall and snowfall events illustrate negative correlations with MP deposition ($r\leq-0.6$) suggesting event occurrence and intensity rather than duration may positively influence MP deposition[21,22]. Despite long durations (≤41 days) represented by the samples, this preliminary dataset suggests that rain, snow and wind events may be drivers in MP deposition at this site. This supports the suggestion by Dris et al.[10] that precipitation events may be a positive driver in atmospheric MP fallout.

The samples collected for the January – March monitoring period contained a visible quantity of orange quartz-like fine dust. This dust presented size (d50 ~8µm), colour and indicative chemical signature descriptive of Saharan dust[23,24] (further details in Supplementary Data). The fine dust, and other particulate matter potentially including some MP particles, are possibly Saharan, North Africa or Iberic sourced material (or potentially sourced along this trajectory)[25]. For example, long-range transport of dust has been shown by van der Does et al.[26] findings of ultra-giant particles (<400µm) traveling trans-oceanic up to 3,500km. The distance MP can travel is currently unknown and further event–based research is needed to identify source and transport vectors of atmospheric MP particles.

Characteristics of MP particles

115 Characterisation was completed following the identification guide presented by Hidalgo-Ruz
116 et al. and Noren et al.[27,28] in conjunction with μRaman analysis. MP particle size or length
117 was defined using the particle characterisation and count functions in ImageJ/FIJI[29],
118 following the method presented by Erni-Cassola et al.[30]. The overall particle size for MP
119 particles are presented in Figure 2, with individual monitoring period sample fragment sizes
120 illustrated in Figure 2b.

121 Figure 2 near here

122 The majority of environmental MP studies that have considered particle size distribution
123 (PSD) illustrate an increasing trend in the number of finer fragments (significantly greater
124 number of MP fragments with smaller particle size)[9,12,31]. The remote atmospheric
125 deposition samples illustrate the majority of identified MP fragments to fall ≤50μm and the
126 overall fragment size trend to follow previous MP particle size trends. When considered
127 relative to the monitoring period (Figure 2b) there is a slight shift in PSD curve that appears
128 to correspond to the fine dust deposition. Samples with no visible quantity of fine dust
129 (November, December) show a greater quantity of smaller fragments. The fine dust laden
130 samples show a small increase in primary fragment size (February-March). It is noted that for
131 the fine dust sample periods there are a greater number of elevated wind periods (wind
132 events >2m/s and greater), higher maximum recorded wind speeds and interspersed periods
133 of calm (wind speed <0.5m/s) that may assist in the conveyance and deposition of the MP
134 fragments.

135 The length of plastic fibres found in the atmospheric fallout samples (Figure 2c) suggests the
136 predominant fibre lengths to be 100-200μm and 200-300μm. Cai et al.[12] found the majority
137 of fibres in Dongguan to be 200-700μm in length with fibres of ≥4200μm (longest fibre),

while Dris et al.[10,11] primarily found fibres of 200-600µm, with the longest recorded fibre ~5000µm. When the scale for fibre length analysis is modified to fit previous studies, the Pyrenees site fibre lengths fall predominantly between 200-700µm (47%) (Cai et al.[12] present ~30% in this predominant category) and 50-200µm (30%) (Dris et al.[10,11] illustrate a higher predominant fibre length of 400-600µm, ~23%). The longest fibre identified as a plastic fibre in this mountain field study was 3000µm. Film size has not specifically been evaluated in previous atmospheric MP analysis so limited comparative information is currently available. Films can be very thin, flat and therefore provide a greater surface area for atmospheric conveyance relative to a fragment of the same mass (Figure 2a and 2d). Within this mountain field study, the predominant film diameter was 50-200µm, larger than the predominant fragment size.

Raman spectroscopic analysis provides a verification of fragments, fibres and films as plastic[31] and characterisation of plastic type (Figure 1). The predominant plastic found in the samples is polystyrene (PS) (as fragments), closely followed by polyethylene (PE). PS and PE are used in many single use plastic items and in packaging material. Approximately 40% of plastic demand is for plastic packaging and PS or PE products[32]. PS and PE are recyclable products, however the European recycling rate is currently ~31% overall (all plastics) and ~41% for plastic packaging (2016[32]) with 3.4Mt of plastic packaging disposed in EU landfill. PE has a low density compared to other plastics, 0.92-0.97g/cm[27] and is a common film plastic (including plastic bags)[33]. PS is a common packaging material having thermal insulating features and the ability to provide both strong and light weight plastic products. PS has a higher density than PE, 0.96-1.1g/cm[3,27] however it is often used in a foam form for packaging, insulation and protection, resulting is a significantly lowered density. Polypropylene (PP) comprises 18% of the identified plastic particles (fibres primarily PP and

PET). PP is used in packaging, textiles and re-usable products. It is the least dense of all plastics (0.9-0.91g/cm^3)[27] and due to its use in textile industry is constructed as fibres as well as objects or films.

The composition of plastic fallout varies over the monitoring period. Initial correlation analysis does not indicate any strong, significant correlations between plastic type and recorded meteorology (rainfall, snowfall, wind speed or events). The complexity of the plastic composition may be due to the source of plastic particles (and therefore wind direction, wind strength), the occurrence of storm events and the duration of calm days relative to event occurrence. The initial consideration of atmospheric MP fallout to meteorological conditions does not suggest a simple meteorological mechanism driving specific or preferential plastic deposition at this field site but does illustrate PS, PE and PP to be the three greatest contributors to the atmospheric fallout at this location.

Remote MP deposition compared to mega-city MP

The MP deposition recorded at this field site equates to an average daily MP deposition of 365/m^2/day (±69, particles ≥ 5µm). Previous atmospheric fallout monitoring[11,12] undertaken in high density urban areas identified daily fallout of 110(±96) and 53(±38) particles/m^2/day (Paris)[10,34] and 228(±43) particles/m^2/day (36 MP particles/m^2/day confirmed) (Dongguan)[12]. Both the Paris and Dongguan studies counted and analysed particles ≥100µm, ≥50 µm and ≥200µm respectively. If only ≥200µm particles are counted in the remote mountain field samples, this equates to 40(±20) particles/m^2/day, 70% as fibres. The Pyrenees field site MP deposition is comparable to the reported mega-city and suburban atmospheric MP deposition despite the remote and mountainous location of notable distance from urban city development or infrastructure.

185 Both the Paris and Dongguan studies primarily focused on MP fibres. If only fibres are
186 considered, the relative daily MP fibre deposition is 36(±18)fibres/m^2/day ≥100µm, or
187 28(±13)fibres/m^2/day ≥200µm. This is lower but comparable to mega-city average MP
188 counts. The fibre count for the Pyrenean site for MP fibres ≥100µm ranges from 22-62
189 fibres/m^2/day. The Paris mega-city study includes periods of lower MP deposition than seen
190 in this field study (Paris MP deposition range 2-355 MP/m^2/day) potentially due to the
191 greater precipitation quantity and frequency at the Pyrenees field site compared to the Paris
192 study period. It is noted that, in concurrence with the Paris and Dongguan findings, there
193 appears to be no direct correlation between MP deposition and average daily rainfall but
194 that the occurrence of precipitation events (rain or snow) and their specific characteristics,
195 intensity and frequency, may be drivers in atmospheric fallout.

196 The Paris and Dongguan studies MP sample composition differs in plastic type as well as
197 shape to this study's findings. PS and PE form a large portion of the plastic type found in the
198 Pyrenees field site. The majority of PS particles were fragments while most fibres were PET
199 or PP. The Pyrenees field study, similarly to the Swiss floodplain findings[7] found MP
200 composition to differ from the city atmospheric findings[11,12]. While acknowledging the
201 different environmental compartment, there have also been several oceanic focused studies
202 that identified high counts of PS alongside PE and PP[35]. Emerging research on the
203 degradation rate of plastics by type suggest that PS, especially EPS, is highly sensitive to
204 mechanical and UV degradation (when compared to PP and PE)[4]. Expanded PS microplastics
205 may be less dense and more easily entrained (therefore transported), and this may help
206 explain the findings at this field site. The composition of plastic waste lost to the
207 environment (not recycled or recovered) is not well documented and this, combined with

208 limited knowledge on degradation rates makes establishing the plastic waste type, shape
209 and size 'escaping' to the environment difficult to quantify or characterise.

210 **Remote atmospheric MP source and transport analysis**

211 Atmospheric MP source and transport analyses are new to MP research. Local to regional
212 transport has been considered for this field site using two methods, a simple MP settling
213 calculation and short-duration Hysplit4 back-trajectory modelling (see Methodology). Back-
214 trajectory duration is defined as ~2hrs (0.1m/s settling velocity[36] for 600m a.g.l. Pyrenean
215 planetary boundary layer depth(PBL)[37]) and each individual wind (>2m/s), rain and snow
216 event has been analysed to provide a spatial context for local MP transport. The simple MP
217 settling calculations, using MP settling velocity, event wind speed and direction and PBL
218 depth[37], provide basic, linear back-trajectories for MP deposited at the field site due to initial
219 entrainment or uplift and horizontal (wind) conveyance (without further mechanical or
220 convective lift). The MP source area or zone of influence defined by this method extends
221 28km north-west to south-west, along the sparsely populated Aulus-les-Bains, Ercé and
222 Massat valleys, over the Guzet-Neige ski fields and south-east along the Vicdessos valley
223 (Figure 3a-b). Wind events >2m/s illustrate a local MP source area across Aulus-les-Bains and
224 the Saint-Girons valleys (42km to the north-west) and 20km to the north-east over Tarascon-
225 sur-Ariège (village populations <6000).

226 Figure 3 near here

227 Hysplit4 back-trajectory modelling allows individual event air parcels to be back-traced
228 illustrating the air parcel trajectory. Using the calculated back-trajectory duration (see
229 Methodology), models for individual rain, snow and wind events were created and collated
230 to provide event-based back-trajectory frequency maps (Figure 3c-e). These short duration

231 back-trajectories include localised updraft, convective mixing and advection, thus extending
232 the MP transport trajectories and the source area 60km to the east, 75km to the west and
233 south and 95km to the north of the site. Hysplit4 MP source areas extend into western
234 Andorra (Andorra le Vella, population ~22,250), the Spanish Pyrenees, the Saint Gaudens
235 valley, across Foix to Muret (population~24,975). However, like the MP settling calculations,
236 they still fall short of the more densely populated and industrialised areas likely to be
237 significant MP emission sources (Toulouse (population ~466,000), Barcelona (population
238 1.6million), Zaragoza (population ~661,000). This dataset does not support long-range
239 transport analysis due to the sampling time-step, however MP emissions are unlikely to be
240 limited to local sources (<100km) due to low local population density.

241 **Evidencing remote atmospheric deposition and transport**

242 This study reports atmospheric deposition of MP in a remote Pyrenean mountain location.
243 The research shows the monitored site received large numbers of MP particles (365 MP
244 particles/m^2/day) in atmospheric deposition collectors over the winter period of 2017-2018.
245 The presented research illustrates the presence of MP in non-urban atmospheric fallout.
246 Analysis for this single site suggests a tentative but possibly important link between
247 precipitation (rain and/or snow), wind speed and direction to MP deposition. Initial local MP
248 trajectory assessment indicates an MP source area extending to 95km from the site,
249 reaching several towns (populations <25,000) but not the city MP emission sources such as
250 Toulouse or Zaragoza. The data cannot prove long-range transport, however air mass
251 trajectory, MP transport and settling considerations suggest MP emission sources to at least
252 be regional (>100km) given the population density within this local area. Longer-distance
253 transport modelling may be possible but requires event specific sampling and back-

trajectory analysis to identify the extent of this transport. It is highly recommended that further monitoring and analysis be undertaken using separate dry and wet deposition sampling equipment. This would advance the understanding of precipitation influence on atmospheric MP deposition and wind trajectory impact on quantity and composition of atmospheric MP fallout.

Data availability. The authors confirm that all data underlying the results presented in this study are available within the Supplementary Information files and can be downloaded in conjunction with this paper.

References

1. Rosevelt, C., Los Huertos, M., Garza, C. & Nevins, H. M. Marine debris in central California: Quantifying type and abundance of beach litter in Monterey Bay, CA. *Mar. Pollut. Bull.* **71**, 299–306 (2013).

2. PlasticsEurope. *Plastics – the Facts 2014 / 2015 An analysis of European plastics production , demand and waste data*. (Plastic Recycling and Recovery Organisations (EPRO), 2015).

3. PlasticsEurope. *Plastics – the Facts 2017, An analysis of the European plastics production, demand and waste data*. (PlasticsEurope, European Association of Plastics Recycling and Recovery Organisations, 2017).

4. Song, Y. K. *et al.* Combined Effects of UV Exposure Duration and Mechanical Abrasion on Microplastic Fragmentation by Polymer Type. *Environ. Sci. Technol.* **51**, 4368–4376 (2017).

5. da Costa, J. P. Micro- and nanoplastics in the environment: Research and policymaking. *Curr. Opin. Environ. Sci. Heal.* **1**, 12–16 (2018).

6. Mattsson, K., Hansson, L.-A. & Cedervall, T. Nano-plastics in the aquatic environment. *Environ. Sci. Process. Impacts* **17**, 1712–1721 (2015).

7. Scheurer, M. & Bigalke, M. Microplastics in Swiss floodplain soils Microplastics in Swiss floodplain soils. (2018). doi:10.1021/acs.est.7b06003

8. Hurley, R., Woodward, J. & Rothwell, J. J. Microplastic contamination of river beds significantly reduced by catchment-wide flooding. *Nat. Geosci.* **11**, 251–257 (2018).

9. Gasperi, J. *et al.* Microplastics in air: Are we breathing it in? *Curr. Opin. Environ. Sci. Heal.* **1**, 1–5 (2018).

10. Dris, R. *et al.* A first overview of textile fibers, including microplastics, in indoor and outdoor environments. *Environ. Pollut.* **221**, 453–458 (2017).

11. Dris, R., Gasperi, J., Saad, M., Mirande, C. & Tassin, B. Synthetic fibers in atmospheric fallout: A source of microplastics in the environment? *Mar. Pollut. Bull.* **104**, 290–293 (2016).

12. Cai, L. *et al.* Characteristic of microplastics in the atmospheric fallout from Dongguan city, China: preliminary research and first evidence. *Environ. Sci. Pollut. Res.* **24**, 24928–24935 (2017).

13. Corcoran, P. L. Environmental Science Processes & Impacts Benthic plastic debris in marine and fresh water environments. *Environ. Sci. Process. Impacts* **17**, 1363–1369 (2015).

14. Zbyszewski, M., Corcoran, P. L. & Hockin, A. Comparison of the distribution and degradation of plastic debris along shorelines of the Great Lakes , North America. *J. Great Lakes Res.* **40**, 288–299 (2014).

15. Zhang, K. *et al.* Microplastic pollution of lakeshore sediments from remote lakes in Tibet plateau, China. *Environ. Pollut.* **219**, 450–455 (2016).

16. Watkins, L., McGrattan, S., Sullivan, P. J. & Walter, M. T. The effect of dams on river transport of microplastic pollution. *Sci. Total Environ.* (2019). doi:https://doi.org/10.1016/j.scitotenv.2019.02.028

17. Centre d'Etudes Spatiales de la BIOsphere (CESBIO). Donnees meteorologiques – Sud Ouest Bernadouze. (2018). Available at: http://www.cesbio.ups-tlse.fr/data_meteo/index.php?perma=1319145390.

18. INSEE. Institut national de la statistique et des etudes economiques. (2018). Available at: https://www.insee.fr/fr/statistiques/3293086?geo=COM-09334. (Accessed: 24th June 2018)

19. Araujo, C. F., Nolasco, M. M., Ribeiro, A. M. P. & Ribeiro-Claro, P. J. A. Identification of microplastics using Raman spectroscopy: latest developments and future prospects. *Water Res.* **142**, 426–440 (2018).

20. Zwaaftink, C. D. G. *et al.* Temporal and spatial variability of Icelandic dust emissions and atmospheric transport. *Atmos. Chem. Phys.* 10865–10878 (2017). doi:10.5194/acp-17-10865-2017

21. Camarero, L., Bacardit, M., de Diego, A. & Arana, G. Decadal trends in atmospheric deposition in a high elevation station: Effects of climate and pollution on the long-

range flux of metals and trace elements over SW Europe. *Atmos. Environ.* **167**, 542–552 (2017).

22. Marticorena, B. *et al.* Mineral dust over west and central Sahel: Seasonal patterns of dry and wet deposition fluxes from a pluriannual sampling (2006-2012). *J. Geophys. Res. Atmos.* **122**, 1338–1364 (2017).

23. Morales-Baquero, R., Pulido-Villen, E. & Reche, I. Chemical signature of Saharan dust on dry and wet atmospheric deposition in the south-western Mediterranean region. *Tellus Ser. B* **1**, 1–12 (2013).

24. Schwikowski, M., Seibert, P., Baltensperger, U. & Gaggeler, H. W. A study of an outstanding Saharan dust event at the high-alpine site Jungfraujoch, Switzerland. *Atmos. Environ.* **29**, 1829–1842 (1995).

25. Dessens, J. & Van Dinh, P. Frequent Saharan Dust Outbreaks North of the Pyrenees: A sign of a climatic change? *Weather* **45**, 327–333 (1990).

26. van der Does, M., Knippertz, P., Zschenderlein, P., Giles Harrison, R. & Stuut, J.-B. W. The mysterious long-range transport of giant mineral dust particles. *Sci. Adv.* **4**, (2018).

27. Hidalgo-Ruz, V., Gutow, L., Thompson, R. C. & Thiel, M. Microplastics in the marine environment: A review of the methods used for identification and quantification. *Environ. Sci. Technol.* **46**, 3060–3075 (2012).

28. Noren, F. *Small plastic particles in Coastal Swedish waters*. *N-Research, KIMO Sweden* (2007).

29. Schindelin, J. *et al.* Fiji: an open-source platform for biological image analysis. *Nat.*

Methods **9**, 676–682 (2012).

30. Erni-Cassola, G., Gibson, M. I., Thompson, R. C. & Christie-Oleza, J. A. Lost, but Found with Nile Red: A Novel Method for Detecting and Quantifying Small Microplastics (1 mm to 20 µm) in Environmental Samples. *Environ. Sci. Technol.* **51**, 13641–13648 (2017).

31. Schymanski, D., Goldbeck, C., Humpf, H. U. & Fürst, P. Analysis of microplastics in water by micro-Raman spectroscopy: Release of plastic particles from different packaging into mineral water. *Water Res.* **129**, 154–162 (2018).

32. European Comission. A European Strategy for Plastics in a Circular Economy. *Eur. Com.* 24 (2018). doi:10.1021/acs.est.7b02368

33. Magnusson, K. *et al.* Swedish sources and pathways for microplastics to the marine environment. A review of existing data. *IVL Rep.* 1–89 (2016).

34. Dris, R. *et al.* Beyond the ocean: Contamination of freshwater ecosystems with (micro-) plastic particles. *Environ. Chem.* **12**, 539–550 (2015).

35. Shim, W. J., Hong, S. H. & Eo, S. Chapter 1 - Marine Microplastics: Abundance, Distribution, and Composition. in *Microplastic Contamination in Aquatic Environments* (ed. Zeng, E. Y.) 1–26 (Elsevier, 2018). doi:https://doi.org/10.1016/B978-0-12-813747-5.00001-1

36. Zender, C. S. Mineral Dust Entrainment and Deposition (DEAD) model: Description and 1990s dust climatology. *J. Geophys. Res.* **108**, 4416 (2003).

37. Sanchez, E., Yague, C. & Gazetner, M. A. Planetary boundary layer energetics simulated from a regional climate model over Europe for present climate and climate

change conditions. *Geophys. Res. Lett.* **34**, (2007).

Acknowledgments

The data has been funded and provided by the CNRS TRAM Project, ANR-15-CE01-0008, Observatoire Homme-Milieu Pyrénées Haut Vicdessos - LABEX DRIIHM ANR-11-LABX0010 and CESBIO. The research leading to these results has also received funding from the People Programme (Marie Curie Actions) of the European Union's Seventh Framework Programme (FP7/2007-2013) under REA grant agreement n. PCOFUND-GA-2013-609102, through the PRESTIGE programme coordinated by Campus France. The authors would like to acknowledge that this work was carried out in the CMAC National Facility, housed within the University of Strathclyde's Technology and Innovation Centre, who are funded with a UKRPIF (UK Research Partnership Institute Fund) capital award, SFC ref. H13054, from the Higher Education Funding Council for England (HEFCE).

Author contributions

SA and DA designed the study, undertook all analysis and co-authored the manuscript. GLR and VRF provided study design and analytical guidance and assisted preparation and revision of the manuscript. PD undertook all field sampling and field protocol design, assisted in sample preparation and contributed to the manuscript. AS, SB and DG provided financial support and field site access that enabled this study to occur and contributed to the manuscript.

Corresponding Author: The corresponding author for correspondence and requests for materials relating to this paper is Dr D Allen, deonie.allen@ensat.fr.

Competing interests: The authors declare no competing interests.

Figure Cations

Figure 1. MP occurrence, MP type, recorded local rain and snow fall for the monitored period, wind speed and wind events. See supplementary information for comment on the fragment, fibre and film ratio. The types of plastics found in the atmospheric fallout derived from Raman spectroscopy analysis, SpectraGryph© spectral analysis software and libraries[44-48]. The plastic types are presented as abbreviations: PS (polystyrene); PE (polyethylene); PP (polypropylene); PVC (polyvinyl chloride); PET (polyethylene terephthalate); other (uncharacterised).

Figure 2. Deposited MP characterisation. (a) and (b) illustrate the particle size distribution for the MP particles identified in the monitoring period. (c) illustrates the range and predominant fibre lengths. (d) illustrates the average diameter of films collected in the rain and snow collectors during the monitoring periods

Figure 3. MP transport trajectories relative to recorded meteorology (simplistic MP settling velocity trajectory calculation, Methodology Eqn.4) and Hysplit4 back-trajectory modelling. Figure 3a illustrates the rain (n=165) and snow (n=186) event trajectories calculated from the maximum recorded wind speed and wind direction of each storm. Figure 3b illustrates the trajectories of wind events >2m/s (n=197). Figure 3c-e present the Hysplit4 back-trajectory model results for each individual rain, snow or wind event >2m/s. The results have been collated and are presented as trajectory frequency graphs. The wind direction data is presented in reference to local populated areas to provide spatial reference.

Methods

Field sampling and data collation

The field site meteorology and sample station was visited five (5) times over the five (5) month monitoring period for acquisition of samples from atmospheric fallout collectors. The sampling period extended over 2017-2018 from November to March. Samples were ideally collected every 4 weeks but due to climatic conditions restricting access the sample periods for the five samples were inconsistent (sample durations: 12, 19, 34, 41 and 34 days respectively for samples November to March). Field blanks were also collected. During this period two independent atmospheric deposition collectors were active at the site. The first collector was a Palmex Rain Sampler (RS1) with a sampling area of 0.014m^2 (dia. 135mm) (constructed of UV resistant PVC and stainless steel). The second collector installed and sampled from was a NILU Particulate Fallout Collector (p.n.o 9721) with a sampling area of 0.03m^2 (dia. 200mm) (constructed of HDPE and stainless steel). Both collectors were open to the atmosphere for the total period of sampling therefore all samples are a combination of dry and wet atmospheric fallout. The samples collected from each atmospheric fallout collector were kept separate (both during field sampling and laboratory sample preparation) thus providing a duplicate sample dataset for each monitoring period.

During collection of the sample material (and all times when near the sampler) all persons were careful to remain down-wind of the sampler, samples exposure time was kept to a minimum and wherever possible cotton clothing was worn to minimise contamination. The total sample volume was collected (without subsampling). Samples from the Palmex collector were decanted into clean glass 2L bottles in the field capped and transported back to the laboratory. The field sample container from the NILU collector was capped and transported back to the laboratory where samples were decanted into clean glass 2L bottles in the laboratory ‘clean room’. All decanted samples were stored in a dark walk-in refrigerator (at 4 deg C) until filtration and sample processing commenced.

In conjunction with physical atmospheric samples wind, humidity, temperature, rainfall and snowfall data was recorded at the monitoring site by the CESBIO meteorological gauging station [17]. This dataset provided local microclimate information at a 30 minute time-step.

Sample processing preparation for MP analysis

All samples (2 x 5 field samples) contained varying amounts of organic and inorganic matter including biofilm and dust. To aid analysis it is necessary to remove as much of the biogenic and non-plastic inorganic material as possible without damaging or losing potential plastic particles. It is also necessary to remove biofilm from the plastic prior to µRaman spectroscopy to ensure effective analysis (spectra clarity). To this end, protocols were selected with the minimum physical manipulation, least number of steps and the least aggressive digestion chemicals and temperatures possible whist achieving the desired results. Sample material was filtered through a 0.45µm PTFE 47mm diameter membrane (Whatman) using borosilicate laboratory glass filtration equipment and vacuum dried with ethanol (96%.vol). Filters were examined and photographed under a stereo microscope Olympus SZX10 with an Olympus SC30 camera attachment (and visually checked using an Axiostar Plus (x50) microscope) to record as much detail of potential plastic particles as possible prior to digestion. The filter was then rinsed into borosilicate glass test tubes with 10ml hydrogen peroxide (H_2O_2) 30%w/w, capped with glass stoppers, and placed in a static heat block (thermomix) at 55°C for 7 days (no agitation). On day 8 a further 5ml of H_2O_2 30%w/w was added to each sample and the sample was left for a further 7 days. H_2O_2 was chosen as the digestion medium as used by previous studies [7,30,38,39] however given the low usage temperature of some plastics (PS=70°C PVC=60°C)[40] and risk of glassing or melting at elevated temperatures, the temperature was purposefully maintained below 60°C to ensure the methodology did not affect the characterisation or result in loss of material.

On day 14 the sample was filtered onto a 0.45µm PTFE 47mm dia. filter membrane, rinsed with 250ml MilliQ (18 MΩ.cm) water and dried with ethanol (96%.vol). Filtered material was then rinsed

454 into density separation glassware with zinc chloride (technipur $ZnChl_2$) at 1.6g/ml density. This was
455 gently agitated (60rpm) for 7 days at room temperature (Edmund Buhler KS-15 shaker). Settled
456 material was drained away with the sediment removal valve and remaining sample filtered onto
457 0.2µm, 25mm dia. aluminium oxide filters (Andodisc^{TM} 25). Glassware was triple rinsed onto the filter
458 with pH4 buffer. The filter was then rinsed with 250ml MilliQ water and vacuum dried with ethanol.
459 The resulting filter was then examined and photographed again to look for changes in either the
460 number of particles or particle character. Whilst it is difficult to quantify particles pre-digestion (due
461 to excessive organic/inorganic material) many of the particles photographed previously were
462 identifiable and any visible change in the material was noted, thus we are confident that the
463 protocols were sufficiently gentle to ensure minimal losses of material.

464 **Blank test**

465 Two sets of laboratory blanks were created in support of this sample preparation process. Two MilliQ
466 samples of 1L, instead of field sample material, were put through the full digestion and zinc chloride
467 separation process, resulting in two full-process blanks (following in detail the process outlined for
468 the sample preparation).

469 A further two laboratory blanks (MilliQ water samples) underwent the digestion process but were
470 filtered onto the Anodisc^{TM} 25 filters without zinc chloride separation. The purpose of these blanks
471 was to help quantify the possible MP contamination resulting from the sampling and sample
472 preparation process.

473 Field blanks were also collected from each collector. Sample collection containers (glass) were taken
474 out on site, connected to and opened at the sample location and then returned to the laboratory.
475 These 'empty' glass containers were then thoroughly rinsed with MilliQ water and the resulting
476 water processed without zinc chloride separation, following the preparation described above.

The blank test resulted in a total of 6 blank samples, 2 from the complete preparation and ZnCl2 process and 4 without ZnCl2 separation (n = 6). The blank filters identified on average 3 (±1) fibres, 1 (±1) film and 8 (±1) fragments per filter.

Visual and ImageJ/FIJI particle inspection and count

All filters were visually inspected under a stereo microscope for MP particles using the identification criteria published by Hidalgo-Ruz (2012), Löder and Gerdts (2015), Norén (2007) [27,28,41]. It is noted that using visual identification alone is not recommended for MP < 500µm, a second technique (FTIR, Raman) is recommended to confirm for small particles [27,28,41,42]. Plastic particulates are visually identified by their shape and colour. Plastics must have no biogenic (cellular) structure; fibres are expected to have a relatively even or consistent thickness along the fibre length and illustrate three dimensional bending; fragments and films are expected to have relatively homogeneous colouring and illustrate a level of transparency or clarity [28,41]. Aged plastic, such as expected in environmental samples, are described by Hidalgo-Ruz (2012)[27] as presenting embrittled and weathered surfaces, to have irregular shapes with broken and sharp edges. Weathered plastics may also show pitting. Colour is also a plastic identifier [27,41], ranging from transparent and variations of white to bright orange, blues, greens and purples through to black. It is noted that biogenic material becomes bleached during the sample preparation process (H_2O_2 digestion) making plastic particulates with colour highly visible and differentiated from residual (post-digestion) biogenic material.

An initial, indicative fragment, fibre and film count was visually undertaken for each sample using an Olympus SZX10stereo microscope. Three locations of 13mm^2 were randomly selected and investigated on each filter (two filters per sample) (random selection to minimise bias) (Peeken 2018). Following the visual identification methodology, a count of plastic fragments, fibres and films was undertaken (n = 6 inspected areas for each sample, total of 254 MP identified). Identification was conservative with a focus on obvious coloured particulates, resulting in a possible under estimation overall due to limited count or testing of white and non-transparent materials.

All filters were then photographed using a Leica DM6000M confocal microscope with a Marzhauser Scan 130/85-4mm X-Y motorised stage. Photographs were manually focused for each frame using a x10 lens. Filters were photographed using the automated mosaic software (Leica proprietary software) and automatically stitched to provide a multistep mosaic image for each filter. The visual count was repeated on the photographs and completed using the software ImageJ. Three 13mm^2 photographed areas of each filter were imported into ImageJ. Particle counts were undertaken using the protocol defined and used by Erni-Cassola et al. (2017)[30] (ImageJ code provided in Erni-Cassola et al (2017)[30] supplementary material doi: 10.1021/acs.est.7b04512). A second count was undertaken following the same method using a larger area (6 x 58mm^2), providing a visual/ImageJ MP count for 50% of the Anodisc^{TM} 25 filter surface. All identified particles (n = 1147) were sized using ImageJ (as completed in Isobe et al. 2015, Imhof et al. 2016[43,44]), providing a length, width and area appropriate for particle size distribution analysis.

Raman set up and analysis

Confirmation of plastic presence and type was achieved by µRaman (Horiba Scientific Xplora Plus, 50-3200cm^{-1} with a 1.5cm^{-1} resolution, confocal imaging accuracy 0.5 µm) confocal microscope with motorised X-Y stage. µRaman spectroscopy has been used in previous studies to confirm visual and Nile Red fluorescence assisted microplastic quantification in environmental samples[30,41,45–48] and has been shown to be effective in microplastic characterisation down to 1 µm[19]. Three areas of each filter (6 x 13mm^2) were randomly selected and analysed for total plastic presence using the 785nm laser (spatial resolution of 1 µm) and 200-2000cm^{-1} Raman shift range. Spectra were collected using an acquisition time of 15 seconds and 10 accumulations, maximum of 25% power (filter) (general settings: grating of 1200gr_mm and 50µm split, modified to achieve effective spectra results as necessary during analysis). Laser power setting were tested on plastic particles to establish the strength necessary for effective spectra imaging with minimal particulate damage. Laser power of 25% resulted in no visible damage to the plastics and acceptable spectra delineation. Laser power of

50% and 100% result in damage (burning or melting) of the plastic as shown in the Supplementary Note 4 – Images of Raman laser impact on plastic.

Each suspected plastic particle was analysed individually, resulting in a dataset of Raman shift spectra's (n = 245 particulate). Each potential identified MP was analysed twice (at two unique locations on the particle) to confirm the Raman spectra. Where the spectra were unclear or not definitive, a third analysis was undertaken. Samples illustrating three unclear spectra were defined as 'not plastic'. The blank filters were tested to quantify the level of contamination (through sample processing and analysis). A new Anodisc^{TM} 25 filter was also analysed to confirm the background filter spectra. The µRaman spectral analysis provided conformation of visual identification, supporting the extrapolation of visual counts to consider spatial and temporal trends.

Raman Spectra analysis

The open source Spectragryph software and databases[49] were used to analyse µRaman spectral results. Individual evaluation of each spectrum was completed, similar to methods of spectra analysis followed in [45,50,51] in conjunction with [52] which provides a clear definition of chemical and bond spectra peaks.

Statistical analysis

Visual and ImageJ MP counts of all filters were confirmed using µRaman spectrography (11% of the filters were analysed using µRaman, 50% of the filters were inspected visually and with ImageJ). The µRaman confirmed count of MP (#/mm^2) was extrapolated to provide an indication of the quantity of MP per filter and therefore per sample. It is acknowledged that extrapolation from subsampled filters does not provide a definitive MP count and ideally all MP particulates would be counted and confirmed with µRaman analysis. Due to analysis constraints complete filter analysis was not possible.

The calculation of MP per m^2/month (31 days) was calculated through a simple sum of sample area MP counts, scaling using known filter and collector areas and known monitoring period durations. The calculations followed the following simple equations.

$$\bar{X} = \frac{(\sum X_{1-n})}{n} \quad \text{Eqn. 1}$$

$\bar{X}$ = the average MP count for a sample area (13mm^2)

$X_{1, 2, 3}$ = the MP count for a sample area 1, 2, 3 etc. (sample area = 13mm^2)

n = sample area number (6 sample areas were investigated for each sample period)

$$\mu P = \left(\bar{X} \times \frac{Y}{y}\right) - \varepsilon \quad \text{Eqn. 2}$$

μP = total MP count per filter

y = sample area (13mm^2 or 0.000013m^2)

Y = total filter area (346 mm^2 or 0.0003m^2)

ε = sampling error, the number of MP particulates found on the blank samples

$$MP = \left(\mu P \times \frac{1}{a}\right) / d \quad \text{Eqn. 3}$$

MP = MP count per m^2 / day

a = sample area of the atmospheric collector (m^2)

d = duration of the sampling period (days)

The quantity of MP/filter is accepted to be representative of the atmospheric deposition for the monitoring period relative to the collection area (Palmex collector = 0.014m^2, NILU collector = 0.03m^2). Provision of MP quantity/m^2 has been previously published and accepted as a method supporting comparison of multiple studies results[8]. Therefore, the results per monitoring period were normalised for 1 day time period (for comparison to Dris et al.[11] and Cai et al.[12]) and 1 metre square area using the known collector surface areas. The two collectors provide replicate samples for

each sample period and therefore were treated as such. Thus, two independent samples were collected for each sample period, providing 2 Anodisc^{TM} 25 filters, with a total of 6 randomly selected areas analysed for MP resulting a per monitoring period n= 6.

Statistical analysis of the MP counts and characteristics has been purposefully kept to a minimum due to the dataset duration (5 monitoring periods) and the single site case study constraints (it is not considered appropriate to generalise from a single case study), the study is presented as a first indication and presentation of remote MP presence only). Simple correlation analysis between particle counts and meteorological data was completed using R Studio (R version 3.4.1) software and standard significance (p-value), Pearson and Spearman correlation tests used appropriate to the data (CRAN packages hydroGOF, Hmisc, Performance Analytics and subsidiaries).

Bias

Use of a non-automated system in particle counting and analysis will induce a level of human bias in the results. To reduce the potential human bias in the results due to lack of automation, random sampling has been employed on all filter counting and µRaman analysis site selection. MP visual, ImageJ and µRaman analysis has been undertaken in triplicate on all filters to further limit bias and uncertainty in the results. MP identification was completed following an identification protocol that was consistently employed on all areas analysed. The identification protocol was conservative, any particles that did not meet visual identification protocol as described by Hidalgo-Ruz et al.[27] and Norén [28] and or did not provide a clear Raman plastic signature were discounted from the analysis to limit mis-identification and bias.

Local transport trajectory and source area assessment

The recorded wind, rain and snow meteorological data was used to support a local MP transport assessment and to help consider potential source and trajectories of MP relative to the field site. The simple numerical assessment of distance and transport duration of MP particles relative to rainfall events, snowfall events and wind occurrences (events) were calculated using the known field site

elevation, upper elevation of MP entrainment[37], wind speed and assumed settling velocity[36] (based on 25µm dust particle). Once elevated, it was assumed that no further meteorological updraft or conveyance assistance (other than recorded horizontal wind speed and direction) influenced the MP (to provide a simplified assessment of possible MP transport).

$$distance = {back - trajectory\ duration}/{wind\ speed} \quad \text{Eqn. 4}$$

distance = potential horizontal trajectory of MP (m)

back-trajectory duration = the duration MP is airborne (sec); calculated as maximum elevation (600m a.g.l)[37]/ settling velocity (0.1 m/s)[36]

wind speed = maximum recorded wind speed (at the meteorological station) during each rain, snow or wind event (m/s)

The wind direction recorded for the rain, snow and wind events were used in conjunction with the calculated horizontal transport distances to create event specific wind rose maps to spatially illustrate the local MP trajectories. It is acknowledged that this is a highly simplified assessment of potential horizontal transport trajectories and does not take into account the complex atmospheric dynamics of mountain terrain or atmospheric mixing. However, it does provide a first simplified assessment of local MP transport.

HYSPLIT4 analysis

The open source modelling software HYSPLIT[53,54] was used to model the back trajectory of air parcel movement from the field site during the five monitoring periods. HYSPLIT version 4 (HYSPLIT4) was used to download and model global wind/atmospheric meteorology data provided by NOAA (Global Data Assimilation System data) (similarly used in[55–57]). Each rainfall (n=165), snowfall (n=186) and wind event >2m/s (n=197) were individually modelled with the back-trajectory duration defined above (Eqn. 4). The multiple individual trajectories were then collated to create a frequency chart of

621 trajectory potentials across the local area. The source point (deposition location in a back-trajectory
622 model) was set to 43N 1E 100m a.g.l.

623 **Methodology References**

624 38. Digka, N., Tsangaris, C., Kaberi, H., Adamopoulou, A. & Zeri, C. Microplastic Abundance and
625 Polymer Types in a Mediterranean Environment. in *Proceedings of the International*
626 *Conference on Microplastic Pollution in the Mediterranean Sea* (eds. Cocca, M. et al.) 17–24
627 (Springer Water. Springer, Cham, 2018). doi:10.1007/978-3-319-71279-6

628 39. Wang, W., Ndungu, A. W., Li, Z. & Wang, J. Microplastics pollution in inland freshwaters of
629 China: A case study in urban surface waters of Wuhan, China. *Sci. Total Environ.* **575**, 1369–
630 1374 (2017).

631 40. Klein, R. Material Properties of Plastics. in *Laser Welding of Plastics: Materials, Processes and*
632 *Industrial Applications* 3–69 (John Wiley & Sons, 2012). doi:10.1002/9783527636969

633 41. Löder, M. & Gerdts, G. Methodology used for the detection and identification of microplastics
634 – a critical appraisal. in *Marine Anthropogenic Litter* (eds. Bergmann, M., Gutow, L. & Klages,
635 M.) (Springer, Cham, 2015). doi:10.1007/978-3-319-16510-3_8

636 42. Shim, W. J., Hong, S. H. & Eo, S. E. Identification methods in microplastic analysis: a review.
637 *Anal. Methods* **9**, 1384–1391 (2017).

638 43. Isobe, A., Uchida, K., Tokai, T. & Iwasaki, S. East Asian seas: A hot spot of pelagic microplastics.
639 *Mar. Pollut. Bull.* **101**, 618–623 (2015).

640 44. Imhof, H. K. *et al.* Pigments and plastic in limnetic ecosystems: A qualitative and quantitative
641 study on microparticles of different size classes. *Water Res.* **98**, 64–74 (2016).

642 45. Lenz, R., Enders, K., Stedmon, C. A., MacKenzie, D. M. A. & Nielsen, T. G. A critical assessment
643 of visual identification of marine microplastic using Raman spectroscopy for analysis

improvement. *Mar. Pollut. Bull.* **100**, 82–91 (2015).

46. Enders, K., Lenz, R., Stedmon, C. A. & Nielsen, T. G. Abundance, size and polymer composition of marine microplastics ≥10μm in the Atlantic Ocean and their modelled vertical distribution. *Mar. Pollut. Bull.* **100**, 70–81 (2015).

47. Käppler, A. *et al.* Analysis of environmental microplastics by vibrational microspectroscopy: FTIR, Raman or both? *Anal Bioanal Chem* **408**, 8377–8391 (2016).

48. Song, Y. K. *et al.* A comparison of microscopic and spectroscopic identification methods for analysis of microplastics in environmental samples. *Mar. Pollut. Bull.* **93**, 202–209 (2015).

49. Menges, F. Spectragryph – optical imaging software. (2016). Available at: https://www.effemm2.de/spectragryph/.

50. Khashaba, P. Y., Ali, H. R. H. & El-Wekil, M. M. A rapid Fourier transform infrared spectroscopic method for analysis of certain proton pump inhibitors in binary and ternary mixtures. *Spectrochim. Acta Part A Mol. Biomol. Spectrosc.* **190**, 10–14 (2018).

51. Ševčík, R. & Mácová, P. Localized quantification of anhydrous calcium carbonate polymorphs using micro-Raman spectroscopy. *Vib. Spectrosc.* **95**, 1–6 (2018).

52. Lagaron, J. M., Dixon, N. M., Reed, W., Pastor, J. M. & Kip, B. J. Morphological characterisation of the crystalline structure of cold-drawn HDPE used as a model material for the environmental stress cracking (ESC) phenomenon. *Polymer (Guildf).* **40**, 2569–2586 (1999).

53. Draxler, R. R. & Hess, G, D. Hysplit4 modeling system. (2018).

54. Stein, A. *et al.* NOAA's HYSPLIT atmospheric transport and dispersion modeling system. *Bull. Am. Meteorol. Soc.* **96**, 2059–2077 (2015).

55. Su, L., Yuan, Z., Fung, J. C. H. & Lau, A. K. H. A comparison of HYSPLIT backward trajectories generated from two GDAS datasets. *Sci. Total Environ.* **506–507**, 527–537 (2015).

667 56. Ashrafi, K., Shafiepour-Motlagh, M., Aslemand, A. & Ghader, S. Dust storm simulation over
668 Iran using HYSPLIT. *J. Environ. Heal. Sci. Eng.* **12**, 9 (2014).

669 57. Reche, I., D'Orta, G., Mladenov, N., Winget, D. M. & Suttle, C. A. Deposition rates of viruses
670 and bacteria above the atmospheric boundary layer. *ISME J.* (2018). doi:10.1038/s41396-017-
671 0042-4

672

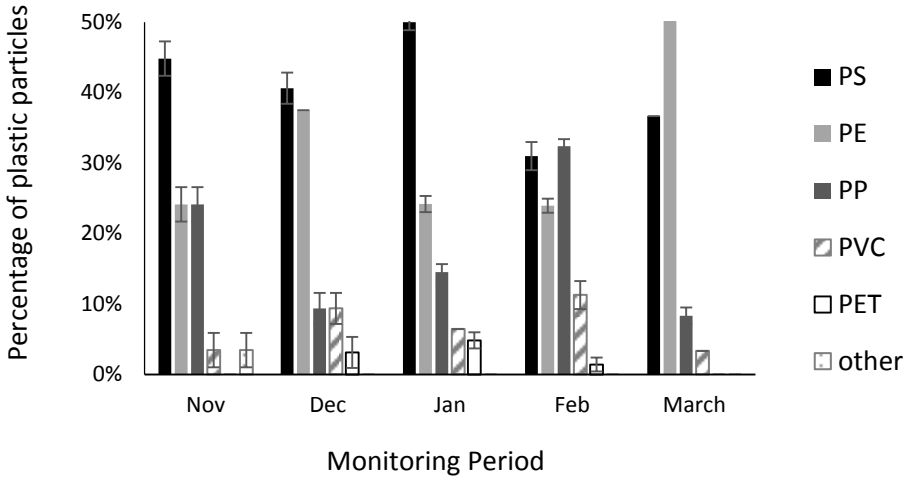
Percentage of plastic particles
50%
40%
30%
20%
10%
0%
Nov
Dec
Jan
Feb
March
Monitoring Period
PS
PE
PP
PVC
PET
other

(b)

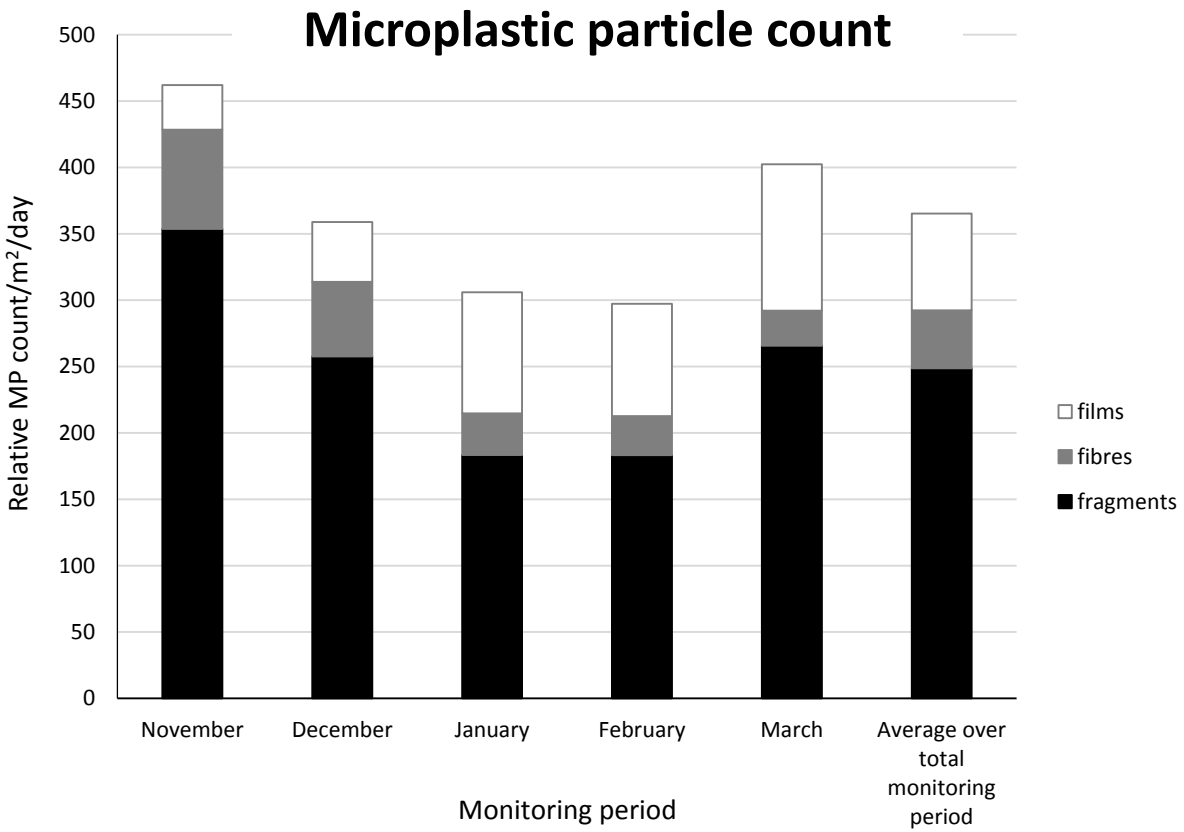
Microplastic particle count
Relative MP count/m²/day
500
450
400
350
300
250
200
150
100
50
0
November
December
January
February
March
Average over total monitoring period
Monitoring period
films
fibres
fragments

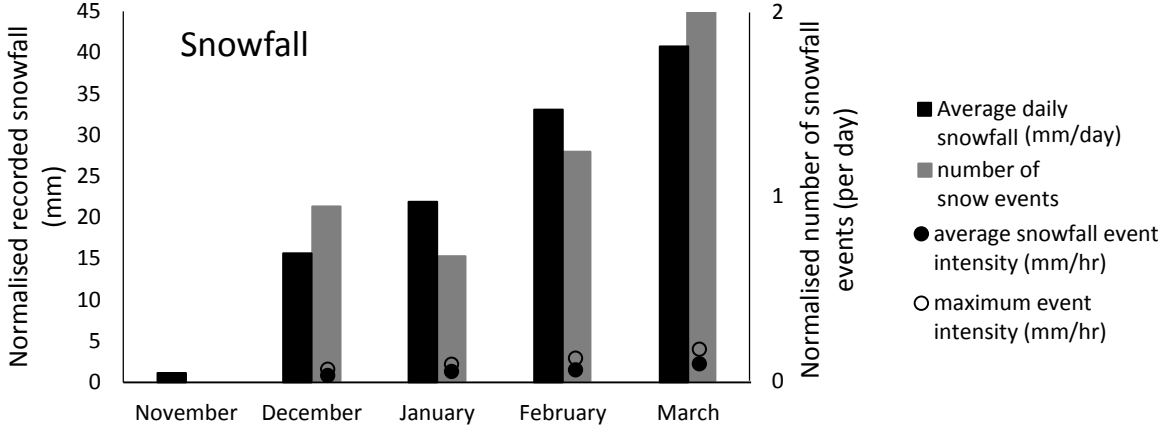
Snowfall
Normalised recorded snowfall (mm)
45
40
35
30
25
20
15
10
5
0
Normalised number of snowfall events (per day)
2
1
0
November
December
January
February
March
Average daily snowfall (mm/day)
number of snow events
average snowfall event intensity (mm/hr)
maximum event intensity (mm/hr)

(d)

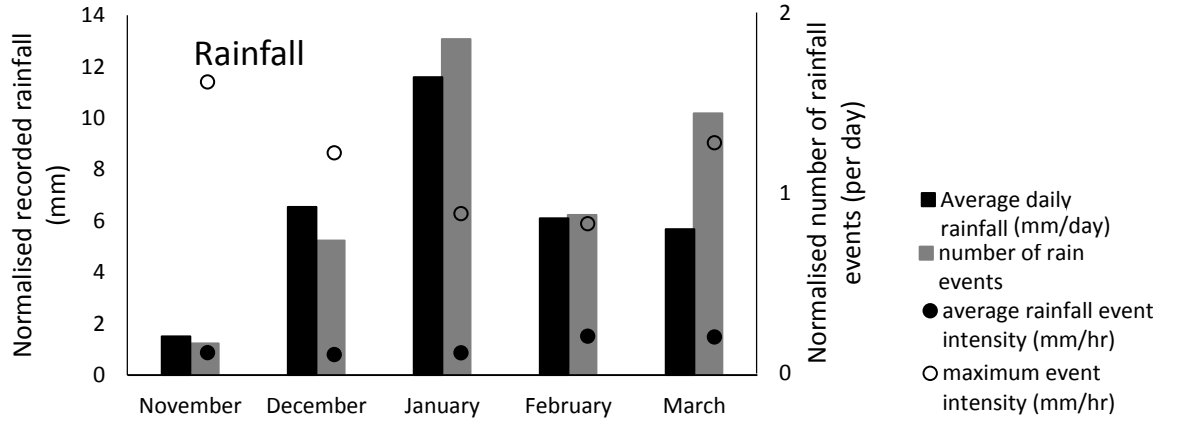
Rainfall
Normalised recorded rainfall (mm)
14
12
10
8
6
4
2
0
Normalised number of rainfall events (per day)
2
1
0
November
December
January
February
March
Average daily rainfall (mm/day)
number of rain events
average rainfall event intensity (mm/hr)
maximum event intensity (mm/hr)

(e)

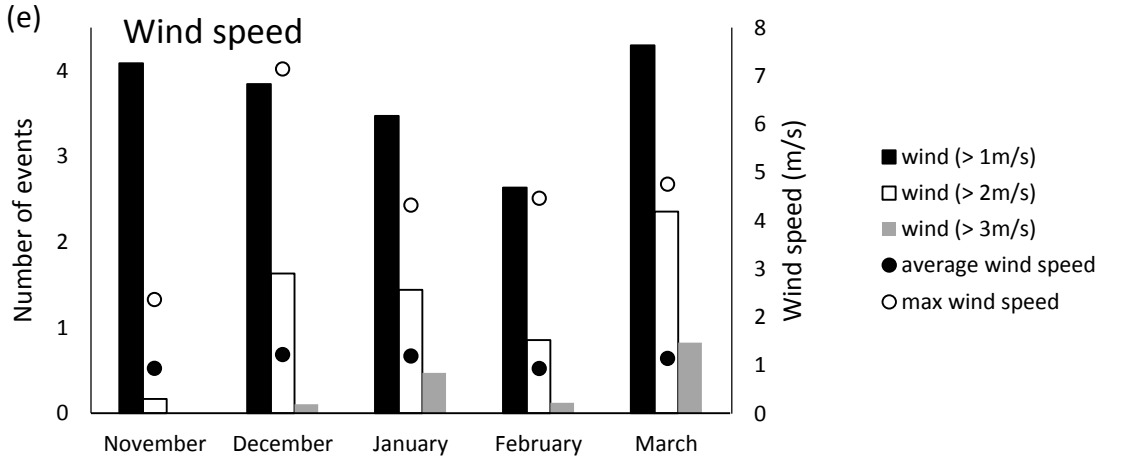
Wind speed
Number of events
4
3
2
1
0
Wind speed (m/s)
8
7
6
5
4
3
2
1
0
November
December
January
February
March
wind (> 1m/s)
wind (> 2m/s)
wind (> 3m/s)
average wind speed
max wind speed

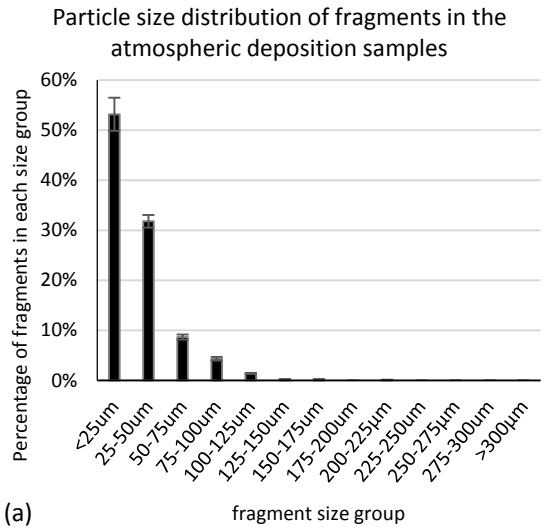
Particle size distribution of fragments in the atmospheric deposition samples
Percentage of fragments in each size group
60%
50%
40%
30%
20%
10%
0%
<25um
25-50um
50-75um
75-100um
100-125um
125-150um
150-175um
175-200um
200-225µm
225-250um
250-275µm
275-300um
>300µm
fragment size group

(a)

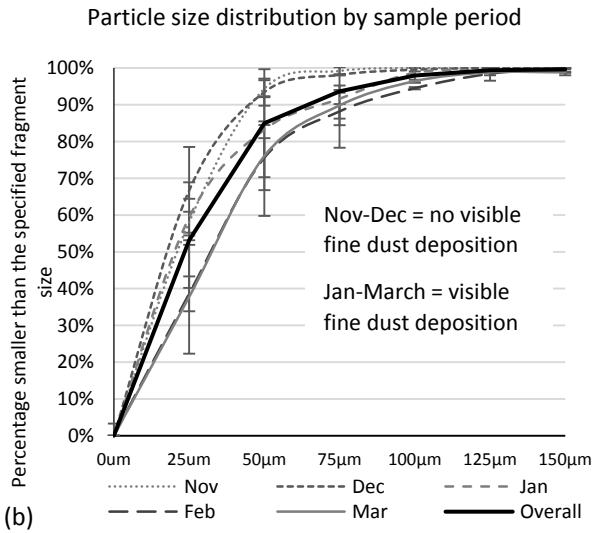
Particle size distribution by sample period
Percentage smaller than the specified fragment size
100%
90%
80%
70%
60%
50%
40%
30%
20%
10%
0%
0um
25um
50µm
75µm
100µm
125µm
150µm
Nov-Dec = no visible fine dust deposition
Jan-March = visible fine dust deposition
Nov
Dec
Jan
Feb
Mar
Overall

(b)

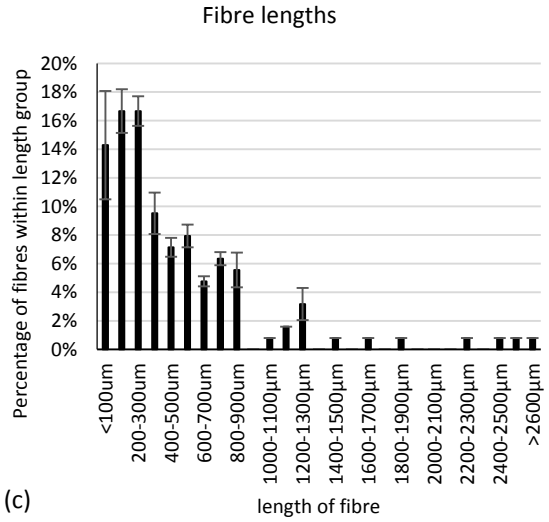
Fibre lengths
Percentage of fibres within length group
20%
18%
16%
14%
12%
10%
8%
6%
4%
2%
0%
<100um
200-300um
400-500um
600-700um
800-900um
1000-1100µm
1200-1300µm
1400-1500um
1600-1700µm
1800-1900µm
2000-2100µm
2200-2300µm
2400-2500µm
>2600µm
length of fibre

(c)

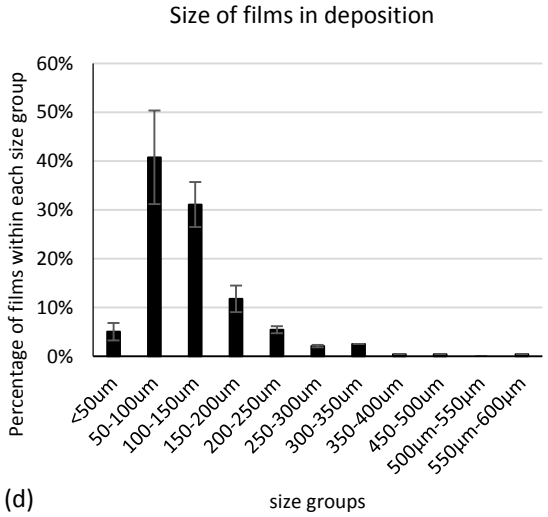
Size of films in deposition
Percentage of films within each size group
60%
50%
40%
30%
20%
10%
0%
<50um
50-100um
100-150um
150-200um
200-250um
250-300um
300-350um
350-400um
450-500um
500µm-550µm
550µm-600µm
size groups

(d)

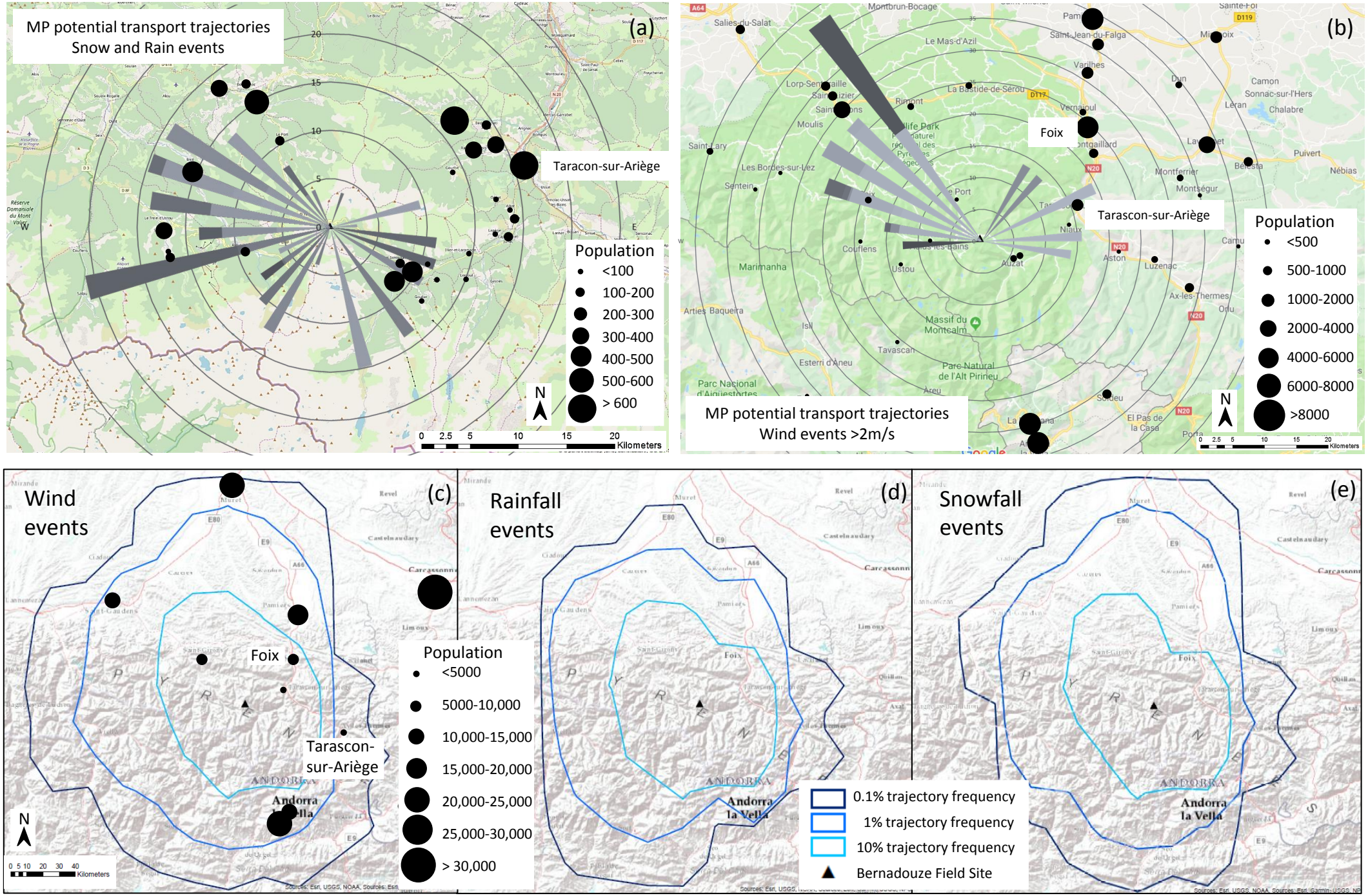
MP potential transport trajectories
Snow and Rain events
(a)
Taracon-sur-Ariège
Population
<100
100-200
200-300
300-400
400-500
500-600
> 600
N
0 2.5 5 10 15 20 Kilometers
(b)
Foix
Tarascon-sur-Ariège
Population
<500
500-1000
1000-2000
2000-4000
4000-6000
6000-8000
>8000
MP potential transport trajectories
Wind events >2m/s
Wind events
(c)
Foix
Tarascon-sur-Ariège
Population
<5000
5000-10,000
10,000-15,000
15,000-20,000
20,000-25,000
25,000-30,000
> 30,000
Rainfall events
(d)
Snowfall events
(e)
0.1% trajectory frequency
1% trajectory frequency
10% trajectory frequency
Bernadouze Field Site